CHEMISTRY
A EUROPEAN JOURNAL

DOI: 10.1002/chem.200903506

Two-Photon Chemistry in Ruthenium 2,2′-Bipyridyl-Functionalized Single-Wall Carbon Nanotubes

Roberto Martín,[a] Liliana Jiménez,[b] Mercedes Alvaro,[a] Juan C. Scaiano,[b] and Hermenegildo Garcia*[a]

Abstract: Ruthenium polypyridyl complexes are widely used as light harvesters in dye-sensitized solar cells. Since one of the potential applications of single-wall carbon nanotubes (SWCNTs) and their derived materials is their use as active components in organic and hybrid solar cells, the study of the photochemistry of SWCNTs with tethered ruthenium polypyridyl complexes is important. A water-soluble ruthenium tris(bipyridyl) complex linked through peptidic bonds to SWCNTs (Ru-SWCNTs) was prepared by radical addition of thiol-terminated SWCNT to a terminal C=C double bond of a bipyridyl ligand of the ruthenium tris(bipyridyl) complex. The resulting macromolecular Ru-SWCNT (≈500 nm, 15.6% ruthenium complex content) was water-soluble and was characterized by using TEM, thermogravimetric analysis, chemical analysis, and optical spectroscopy. The emission of Ru-SWCNT is 1.6 times weaker than that of a mixture of $[Ru(bpy)_3]^{2+}$ and SWCNT of similar concentration. Time-resolved absorption optical spectroscopy allows the detection of the $[Ru(bpy)_3]^{2+}$-excited triplet and $[Ru(bpy)_3]^{+}$. The laser flash studies reveal that Ru-SWCNT exhibits an unprecedented two-photon process that is enabled by the semiconducting properties of the SWCNT. Thus, the effect of the excitation wavelength and laser power on the transient spectra indicate that upon excitation of two $[Ru(bpy)_3]^{2+}$ complexes of Ru-SWCNT, a disproportionation process occurs leading to delayed formation of $[Ru(bpy)_3]^{+}$ and the performance of the SWCNT as a semiconductor. This two-photon delayed $[Ru(bpy)_3]^{+}$ generation is not observed in the photolysis of $[Ru(bpy)_3]^{3+}$; SWCNT acts as an electron wire or electron relay in the disproportionation of two $[Ru(bpy)_3]^{2+}$ triplets in a process that illustrates that the SWCNT plays a key role in the process. We propose a mechanism for this two-photon disproportionation compatible with i) the need for high laser flux, ii) the long lifetime of the $[Ru(bpy)_3]^{2+}$ triplets, iii) the semiconducting properties of the SWNT, and iv) the energy of the HOMO/LUMO levels involved.

Keywords: disproportionation · carbon nanotubes · time-resolved spectroscopy · two-photon process

Introduction

Covalent functionalization of single-wall carbon nanotubes (SWCNTs) is a general tool to prepare macromolecular entities with defined morphology and adequate response.[1–3] These entities represent a bridge between molecules and materials and hold a large promise for development of novel nanometric optoelectronic devices.[4–6] One of the potential applications of SWCNTs is as active components in photovoltaic cells for solar energy conversion.[7–14] For this application, and considering the optical spectra of SWCNT, it is necessary to combine SWCNTs with an appropriate dye to act as light harvester.[8,9,13,15–17] In solar cell technology, ruthenium polypyridyl complexes are the universal dyes to harvest sunlight in dye-sensitized semiconductor solar cells (DSSCs).[18–25] The high efficiency of current DSSCs depends largely on the ability of ruthenium polypyridyl complexes to absorb a broad region of the solar spectrum, leading to a fast and efficient electron injection into the semiconductor conduction band.[18] The unique performance of ruthenium

[a] R. Martín, M. Alvaro, Prof. Dr. H. Garcia
Instituto de Tecnología Química CSIC-UPV
Universidad Politécnica de Valencia
Av. de los Naranjos s/n, 46022 Valencia (Spain)
Fax: (+34) 963-877-809
E-mail: hgarcia@quim.upv.es

[b] Dr. L. Jiménez, Prof. Dr. J. C. Scaiano
Department of Chemistry and
Centre for Catalysis Research and Innovation
University of Ottawa
10 Marie Curie, K1N 5N6, Ottawa (Canada)
Fax: (+1) 613-5625633

polypyridyl complexes as solar-light harvesters has triggered wide interest in exploring the potential of SWCNT covalently tethered to ruthenium polypyridyl complexes in organic or hybrid solar cells. Thus, not surprisingly, one of the SWCNT derivatives that has been explored for hybrid solar cells consists of a ruthenium polypyridyl complex covalently attached to the carbon nanotube.[10, 14, 26–29] One material consisting of a SWCNT with covalently attached ruthenium complexes has already been used in combination with TiO_2 for the preparation of a hybrid solar cell with promising results.[10, 14, 28, 29] However, to understand the process limiting the efficiency, and eventually improve further the performance of SWCNT-based solar cells, one needs to characterize the photochemistry of these ruthenium polypyridyl SWCNT complexes. In particular, it is important to determine which photochemical events take place upon irradiation of well-characterized samples of Ru-SWCNT and if these samples perform similarly or differently than the ruthenium polypyridyl complexes anchored on titania surfaces.[18,19] An additional interest in the ruthenium polypyridyl complexes attached to SWCNT stems from the fact that $[Ru(bpy)_3]^{2+}$ complexes are favored chromophores because their photochemistry is understood in a large variety of homogeneous and heterogeneous systems, as well as in the presence of a wide range of electron acceptors.[30] Therefore, the photochemistry of a system comprising the combination of ruthenium polypyridyl complexes and SWCNT is also of importance from a fundamental point of view, especially considering the current interest in SWCNT-derived materials and the way in which the nanotube interacts with electronically excited chromophores.[31,32] On the other hand, as in many derivatives of SWCNT having a chromophore covalently attached, one specific point is to establish the benefits of having a covalent linkage between the chromophore and the SWCNT compared to a simple mixture of the two components. In the present work we describe the synthesis and photochemistry of a well-defined macromolecule derived from a short, soluble SWCNT, which has a covalently attached ruthenium polypyridyl complex (Ru-SWCNT). One crucial issue relating to SWCNT materials is to provide sufficient structural data to ensure reproducibility and reliability in their preparation and their properties. This includes the purity and morphology of the SWCNT and evidence in support of the success of the covalent anchoring between the chromophore and the nanotube. In this regard, in the one precedent of using a Ru-SWCNT material, no characterization data was provided,[10,29,33] thus limiting the usefulness of the results. Also the electrochemiluminescence of a Ru complex covalently bonded to SWCNT has been recently reported.[34] Herein we have found unique photochemical behavior of Ru-SWCNTs compared to related materials studied so far in terms of the dependence of the photochemistry on the light intensity and on the excitation wavelength. Ru-SWCNT exhibits an unprecedented two-photon photochemistry that arises from a combination of factors including the long-lifetime of the ruthenium-localized exciton, the relative energy of the HOMO/LUMO $[Ru(bpy)_3]^{2+}$ orbitals with respect to the SWCNT, and the ability of the SWCNT as electron conductor. The unique two-photon chemistry observed for Ru-SWCNT is distinctive from the behavior of the individual components and nicely illustrates the novel photonic properties that chromophore-CNT materials can possess.

Results and Discussion

Synthesis of Ru-SWCNT: The key step in the synthetic approach used to covalently join $[Ru(bpy)_3]^{2+}$ complexes and short, soluble SWCNT, is the radical addition of a thiol on a terminal C=C double bond. This reaction occurs in very high yields under mild conditions in the absence of oxygen and without the need of acid, bases, or redox reagents. Owing to the compatibility of the thiol addition to C=C double bonds with many functional groups, the reliability of the process as well as its high yields, this reaction has been widely used to covalently attach organic moieties to insoluble supports including high surface area modified silicas and polymers.[35,36] Based on this convergent strategy we proceeded to prepare an allyl derivative of the Ru polypyridyl complex, as well as a thiol-terminated single-wall carbon nanotube. The synthetic route for the preparation of Ru-SWCNT is shown in Scheme 1.

To prepare the vinyl derivative of the ruthenium complex, we first prepared a 2,2′-bipyridyl ligand, which has a 3-butenyl chain at the 4-position of the 2,2′-bipyridyl. The synthesis of this ligand was accomplished, starting from 4,4′-dimethyl-2,2'-bipyridine by lithiation with lithium diisopropylamine (LDA) and subsequent nucleophilic substitution with allyl bromide. The resulting 4-(3-butenyl)-4′-methyl-2,2′-bipyridine was used as a bidentate ligand to replace chloride in commercially available bis-(2,2′-bipyridine)dichlororuthenium(II).

To prepare thiol-derivatized carbon nanotubes, we started with commercially available high pressure carbon monoxide (HiPCO) SWCNT that was submitted to purification and subsequent shortening of the nanotube by using HNO_3 and sonication, following well-established procedures.[37–40] The resulting short, soluble SWCNT was free from inorganic impurities and carbonaceous materials and was highly soluble in water, forming indefinitely persistent black inks. The average length of these short single-wall nanotubes (500 nm) was determined by using TEM and AFM. This material was submitted to functionalization through peptidic bonds by using 2-mercaptoethylamine. The resulting thiol derivative of SWCNT (SH-SWCNT) has been previously described as a suitably functionalized carbon nanotube for anchoring covalently organic units.[40]

Characterization of Ru-SWCNT: The resultant Ru-SWCNT material was characterized by using electron microscopy, chemical and TGA analyses, and spectroscopic techniques. Analysis of the TEM images reveals a short SWCNT with an average length of 500 nm and a low degree of agglomera-

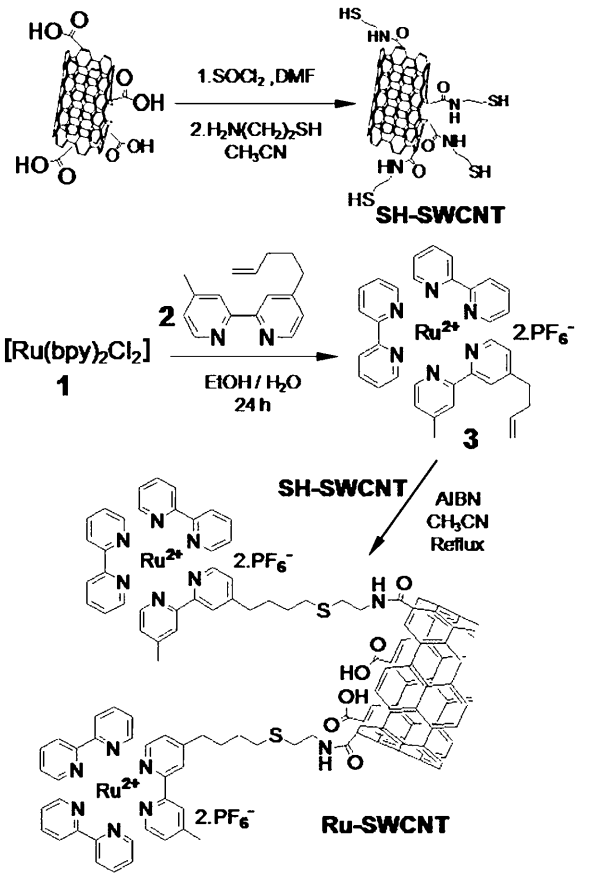

Scheme 1. Route for the synthesis of short SWCNTs functionalized by vinyl ruthenium complexes (Ru-SWCNTs).

tion. Selected representative TEM images obtained for the Ru-SWCNT sample are presented in Figure 1. They show the high quality of our sample, particularly the absence of adventitious particles and carbonaceous material. The average length of Ru-SWCNTs in comparison to the much longer nanotubes present in the original commercial SWCNT samples (several microns), its purity, the presence of oxygenated functional groups on the treated carbon nanotubes, and the presence of highly water-soluble ruthenium polypyridyl units explains the high solubility of the Ru-SWCNT in water ($>10\,mg\,mL^{-1}$).

Thermogravimetric (TG) analysis supports the success of the purification procedure. The profiles of the original SWCNT and Ru-SWCNT are displayed in Figure 2; the raw commercial SWCNT sample (Figure 2a) contains about 50% of the material that does not burn upon heating under an air-flow at 800°C. This residual weight after heating at high temperatures is assumed to correspond to inorganic particles present in the commercial SWNT. In contrast, the TG profile of purified SWCNT (Figure 2b) and SH-SWCNT (Figure 2c) already shows that an almost complete combustion of the material occurs upon heating the sample in air, the residual weight being less than 2.1%. In the case of Ru-SWCNT a different TG profile is observed that indicates the presence of Ru complexes (Figure 2d). Also the percentage

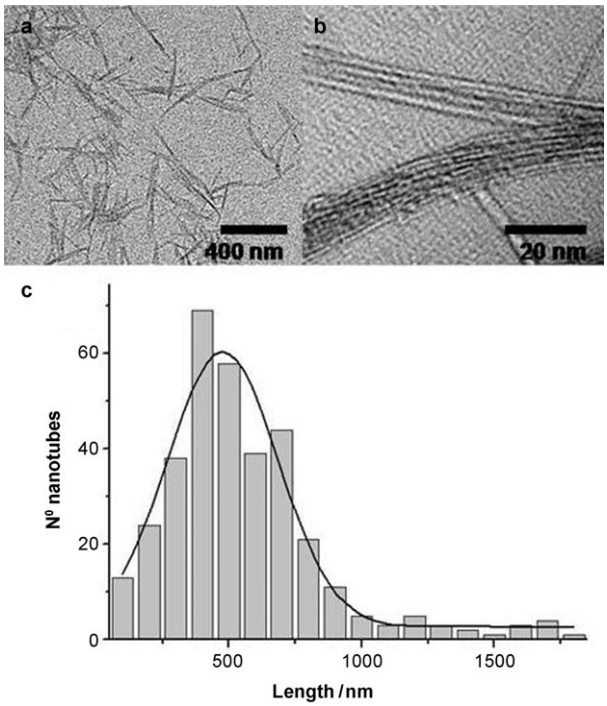

Figure 1. Selected TEM images of a) Ru-SWCNTs and b) the limited bundling of the sample. c) The statistical length distribution graph of the Ru-SWCNTs.

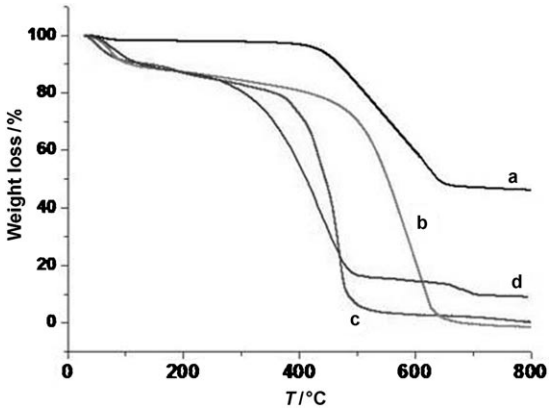

Figure 2. TG profile measured under air of a) raw SWCNT, b) purified short SWCNT, c) SH-SWCNT, and d) Ru-SWCNT. Note the residual weight remaining after combustion, particularly for raw SWCNT and Ru-SWCNT.

of residual weight at 800°C of Ru-SWCNT is 7.5%, that is, higher than that for SH-SWCNT. We attribute the increase in the non-carbonaceous material in Ru-SWCNT to ruthenium oxides arising from the combustion of Ru-SWCNT. Combustion chemical analysis of purified short, soluble SWCNT shows that the sample is free of detectable amounts of nitrogen and sulfur. Upon functionalization with thiol units, the combustion chemical analysis of SH-SWCNT shows the presence of the expected one-to-one nitrogen-to-sulfur atomic ratio in stoichiometric amounts in 0.28 and

0.54 wt%. The presence of N and S in SH-SWNT agrees with the peptidic functionalization. Combustion chemical analysis of Ru-SWCNT also shows an increase in nitrogen content. The experimental N/S atomic ratio of 6.8 determined for Ru-SWCNT is in agreement with an almost complete functionalization of the thiol groups of SH-SWCNT, and indicates that the ruthenium complex loading estimation based on N analysis in Ru-SWCNT is 15.6 wt%. This loading is remarkable considering that in previous occurrences of covalent functionalization of SWCNTs the loadings obtained were around 4 wt%; it is reasonable to anticipate that the ruthenium complex loading can affect the performance of the material with respect to its activity in solar cells.

The presence of ruthenium and its oxidation state in Ru-SWCNT was determined by X-ray photoelectron spectroscopy (XPS). Figure 3 shows the ruthenium(II) $3p_{3/2}$ band ap-

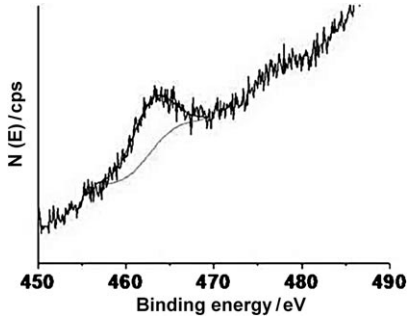

Figure 3. Ru $3p_{3/2}$ region of the X-ray photoelectron spectrum of Ru-SWCNT.

pearing at a binding energy of 463.24 eV. The peak area and the intensity of the signal are in agreement with the loading around 15.6% and with the relatively low sensitivity of the XPS technique. However the binding energy clearly establishes that the oxidation state of ruthenium is 2+. This value is found to be between the ruthenium(0) peak position at about 461 eV and the ruthenium(IV) peak at 465 eV. Therefore, our experimental measured value is in agreement with the 2+ oxidation state of ruthenium in Ru-SWCNT.

Raman spectra of the series of samples are shown in Figure 4, which reveals the expected three characteristic peaks present in the SWCNT corresponding to the tangential vibration at $\tilde{\nu}=1585\ cm^{-1}$ (G), the broader band corresponding to wall defects at $\tilde{\nu}=1285\ cm^{-1}$ (D), and the typical weak radial breathing mode (RBM) peak at $\tilde{\nu}=180\ cm^{-1}$. The relative intensity of the G/D peaks is considered as a parameter related to the presence of wall defects. In the series of spectra shown in Figure 4, it is remarkable that purification and shortening of the SWCNT increases this G/D ratio.

This increase of the G/D ratio indicates that the shortening of the nanotubes occurs at the defect sites in the graphene wall, leading to an apparent healing of the sample. Subsequent functionalization of the purified, short SWCNTs

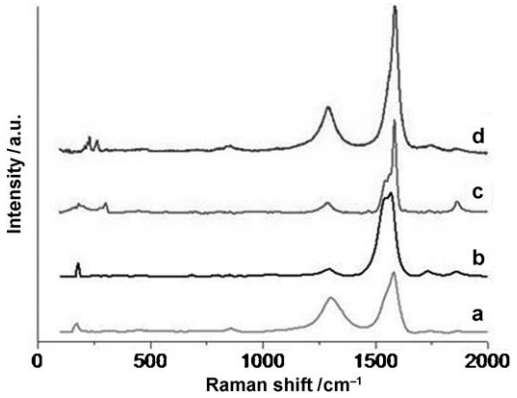

Figure 4. Raman spectra of a) the raw SWCNT, b) the purified short SWCNT, c) the SH-SWCNT, and d) the Ru-SWCNT.

does not change the G/D intensity ratio a great deal, although some sharpening of the G band and shift in the position of the D peak is observed. These facts can be interpreted if you consider that functionalization does not affect the graphene walls and occurs most often at the D sites. With respect to the RBM peak considered as a hallmark specific of the SWCNT, a variation of its position and splitting is observed upon covalent functionalization (Figure 4c,d). This can be interpreted as a reflection of the interaction of the organic moieties with the graphene wall of the nanotube. However alternative explanations exist, particularly preferential functionalization of conducting/semiconducting SWCNT, although this is less likely, in view of the chemical route depicted in Scheme 1, it cannot be ruled out.

Typically Raman spectra do not show any vibration corresponding to the attached subunits. This is generally attributed to the larger intensity of the peaks corresponding to the nanotube at the laser wavelength used for excitation of the sample ($\lambda=785$ nm). In contrast, pristine SWCNTs are almost IR-silent, thus, IR detection of covalently attached units is relatively easy. FT-IR spectroscopy provides information complementary to that obtained by Raman spectroscopy. Figure 5 shows the set of IR spectra recorded for the

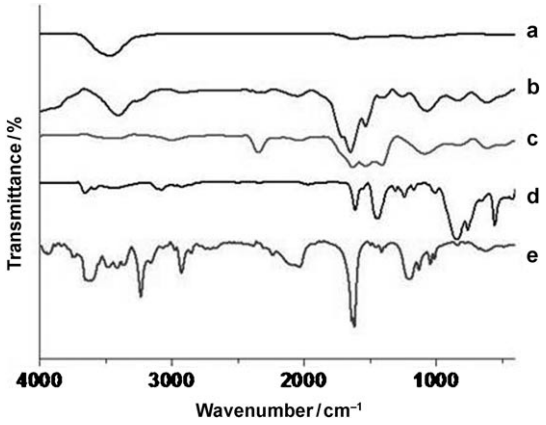

Figure 5. FT-IR spectra of a) the raw SWCNT, b) the purified short SWCNT, c) the SH-SWCNT, d) the vinyl $[Ru(bpy)_3]^{2+}$ derivative, and e) the Ru-SWCNT.

commercial SWCNT to the final Ru-SWCNT. They show that purification and shortening of the SWCNT increases the intensity of the peaks corresponding to OH (3650–3200 cm^{-1}) and C=O (1750–1650 cm^{-1}), indicating the formation of carboxylic acid groups (Figure 5b). Upon formation of the peptidic bonds, the carboxylic acid groups completely disappear and are replaced by the characteristic S–H stretching vibration at $\tilde{\nu}=2300\ cm^{-1}$ (Figure 5c). The IR spectrum of Ru-SWCNT shows the disappearance of the SH bonds and the presence of aromatic and aliphatic CH (1600–1400 cm^{-1} region) as well as an intense C=O peak and aromatic vibrations (Figure 5e). The apparent increase in the intensity of the C=O stretching vibration in the FT-IR spectrum of Ru-SWCNT with respect to SH-SWCNT is probably attributed to the coincidence of the C=O peak with another intense vibration present in the Ru complex.

The remarkable solubility of Ru-SWCNT allowed us to record the ^{1}H NMR spectrum in solution (Figure 6). In

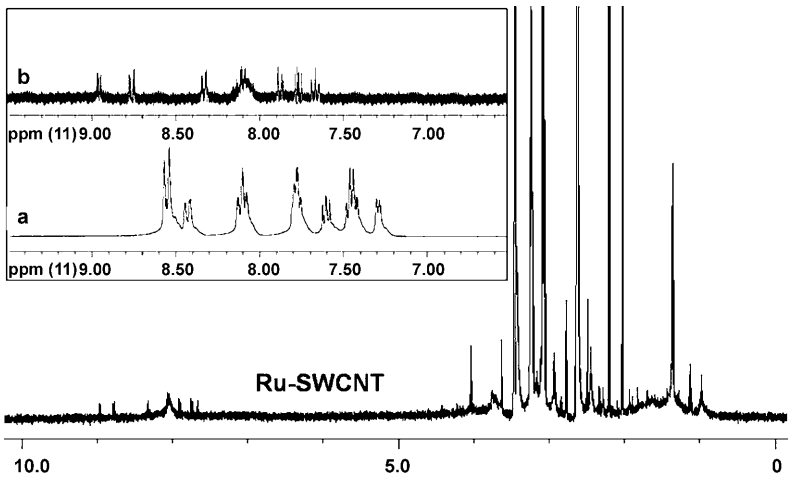

Figure 6. Solution ^{1}H NMR spectrum of the Ru-SWCNT recorded in [D_6]DMSO. The inset shows an expansion of the aromatic protons of a) the ruthenium derivative **2** and b) the Ru-SWCNT.

SWCNT research it is very uncommon to provide NMR data of the SWCNT derivatives after functionalization. However we have recently succeeded in providing credible ^{1}H NMR data in support of the covalent functionalization.[41,42] Furthermore, besides the complex 2.0–3.5 ppm region assigned to solvents, the ^{1}H NMR spectrum of Ru-SWCNT shows the disappearance of the vinylic hydrogens present in the Ru complex used as the precursor and notable variations in the aromatic region. The inset of Figure 6 shows a comparison of the aromatic region of the solution ^{1}H NMR spectrum of the vinylic Ru complex precursor and the resulting Ru-SWCNT. A downfield shift of up to 0.45 ppm is observed for some signals. We interpret these δ shifts as reflecting the anisotropy experienced by the bipyridyl Ru ligands as a result of the proximity of the graphene walls. Particularly important is the fine resolution of the ^{1}H NMR signals that contain structural information supporting the covalent linkage between the Ru complex and the graphene walls.

Altogether the characterization data presented above indicates that the Ru-SWCNT sample under study is constituted of highly soluble, short nanotubes, which have covalently attached ruthenium complex units (15.6%).

Photoluminescence study: It is well known that ruthenium polypyridyl complexes in water exhibit a relatively intense room-temperature phosphorescence emission ($\lambda_{ph}=595$ nm; $\Phi_{ph}=0.042$) upon excitation of the MLCT band ($\lambda_{ex}\approx440$ nm).[44] The phosphorescence lifetime (τ_{ph}) of [Ru(bpy)$_3$]$^{2+}$ in water determined from the best fit of the emission temporal profile to first-order kinetics was 580 ns. We have determined that purified, short SWCNTs quench the phosphorescence of the parent [Ru(bpy)$_3$]$^{2+}$ ion, not covalently bonded in solution, with an apparent quenching constant (k_q) of 6.1×10^5 mL $\mu g^{-1}\,s^{-1}$. Figure 7 shows the quenching of [Ru(bpy)$_3$]$^{2+}$ phosphorescence by SWCNT and the corresponding Stern–Volmer plot from which k_q was obtained.

As expected, in view of the general behavior of [Ru(bpy)$_3$]$^{2+}$, Ru-SWCNT also exhibits phosphorescence ($\lambda_{ph}=$ 602 nm). The emission intensity of Ru-SWCNT is, however, three times lower than that for an optically matched solution of [Ru(bpy)$_3$]$^{2+}$. Moreover, the phosphorescence of Ru-SWCNT is 1.6 times less intense than that from a mixture of [Ru(bpy)$_3$]$^{2+}$ and SWCNT at the same concentrations. The decrease of the emission intensity of Ru-SWCNT compared to the [Ru(bpy)$_3$]$^{2+}$/SWCNT mixture serves to estimate in quantitative terms the influence of the covalent attachment enhancing the interaction between [Ru(bpy)$_3$]$^{2+}$ and SWCNT that is already present (even though somewhat weaker) without the covalent linkage. The phosphorescence lifetime determined for Ru-SWCNT is also different and longer lived ($\tau_{ph}=670$ ns) than that measured for [Ru(bpy)$_3$]$^{2+}$. The longer lifetime can reflect the less polar environment experienced by the residual population of the still emissive ruthenium complex on the vicinity of the SWCNT with respect to water.

In this way, covalent attachment of [Ru(bpy)$_3$]$^{2+}$ to the SWCNT does not introduce a new property, but increases the strength of interaction between [Ru(bpy)$_3$]$^{2+}$ and SWCNT by reducing the diffusional freedom and by maintaining [Ru(bpy)$_3$]$^{2+}$ and SWCNT in close proximity. The tethering also provides some protection of the [Ru(bpy)$_3$]$^{2+}$ ion from the solvent.

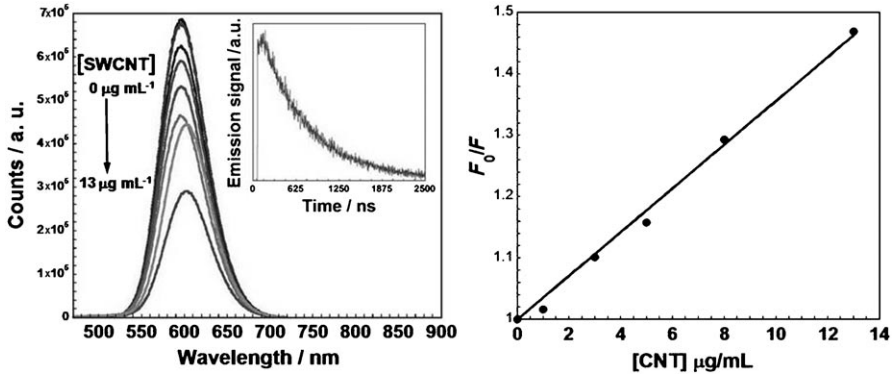

Figure 7. Phosphorescence quenching of the parent $[Ru(bpy)_3]^{2+}$ in water by SWCNTs and the corresponding Stern–Volmer plot from which k_q was obtained. The inset shows the temporal profile of the photoluminescence monitored at $\lambda = 600$ nm in water upon excitation at $\lambda = 440$ nm.

Transient absorption spectroscopy: The previous phosphorescence study proves the interaction of ruthenium polypyridyl triplets with the SWCNT, but does not give indication of the quenching mechanism and the nature of the intermediates involved. In contrast, time-resolved absorption spectroscopy can provide information about the nature of the quenching process.[45]

Considering the visible absorption band of the ruthenium complex, a tunable OPO laser operating from $\lambda = 430$ to 550 nm was used as the excitation light. The power of the excitation pulse was constant (10 mJ pulse^{-1}) when the excitation wavelength was varied. Owing to the intense phosphorescence occurring from $\lambda = 520$ to 800 nm and that the reported absorption spectra of $[Ru(bpy)_3]^{2+}$ triplets ($\lambda = 360$ and 420 nm) and $[Ru(bpy)_3]^{+}$ ($\lambda = 360$, 500, and 550 nm) have in common an absorption band around $\lambda = 360$ nm, the transient signal was initially monitored at this common wavelength.[46,47] As anticipated, considering the ground-state MLCT absorption band of the $[Ru(bpy)_3]^{2+}$ complex from $\lambda = 400$ to 500 nm and peaking at $\lambda = 490$ nm, the intensity of the signal varies with the excitation wavelength following the response expected for excitation of the MLCT of the $[Ru(bpy)_3]^{2+}$ chromophore of Ru-SWCNT.

The maximum intensity of the signal was recorded for $\lambda =$ 490 nm laser excitation in agreement with the MLCT λ_{max} for the $[Ru(bpy)_3]^{2+}$ subunit of a Ru-SWCNT. Figure 8 shows the transient signals (not-normalized) recorded for Ru-SWCNT, as a function of the excitation wavelength in the range $\lambda = 430$–550 nm and a table of the top ΔO.D. values and a description of the signal profile monitored at 360 nm.

Besides the intensity variations, the remarkable changes observed in the temporal profile of the 360 nm signal, as a function of the excitation wavelength (Figure 8), were totally unexpected; upon excitation of the MLCT band of the $[Ru(bpy)_3]^{2+}$ subunit, the signal rises instantaneously and decays in the first 500 ns after the laser pulse (region A in Figure 8), followed by a growth from 500 to 1000 ns (region B), and a final decay (region C). This temporal profile requires more than a single species to be interpreted.

Considering the lifetimes of the possible transient absorbing at the monitoring wavelength species, a reasonable assignment is to attribute the region A to the decay of the triplet exciton localized in the $[Ru(bpy)_3]^{2+}$ chromophore, and the subsequent regions B and C to the growth and decay of $[Ru(bpy)_3]^{+}$ that will be generated with a delay after the laser pulse.

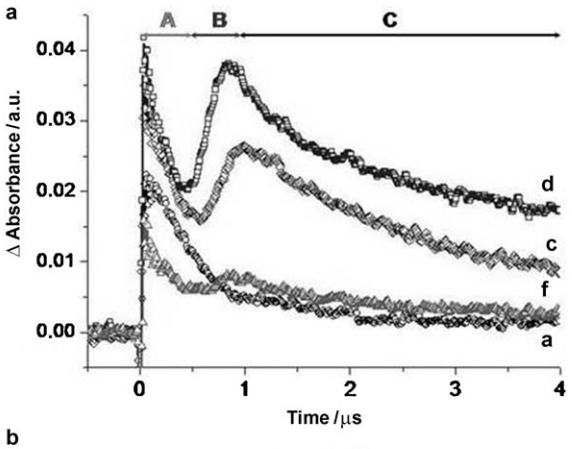

b

λ_{ex} / nm	TOP O.D. / a.u.	Signal kinetics
a) 430	0.0223	First order
b) 450	0.0194	First order
c) 470	0.0349	Decay-Growth-Decay
d) 490	0.0417	Decay-Growth-Decay
e) 510	0.0359	Decay-Growth-Decay
f) 530	0.0232	Decay-Growth-Decay
g) 550	0.0159	First order

Figure 8. a) Transient signals (not-normalized) of a N_2-purged solution of Ru-SWCNT in water (70 mg mL^{-1}) recorded at different laser excitation wavelengths. The temporal profiles (a, c, d, and f) were selected from the table (b), which shows the top optical density (O.D.) (absorbance) and features of the profiles recorded upon excitation of Ru-SWCNT with an OPO laser every 20 nm.

The transient spectra recorded at several time delays after the 490 nm laser pulse is characterized by a continuous absorption spanning the complete wavelength range, very similar to those previously observed in the laser flash photolysis of other chromophore-SWCNTs such as azaxanthone covalently attached to a SWCNT.[43] In addition to this continuous absorption, some weaker features in the regions $\lambda =$

350–390 and 500–600 nm compatible with the absorption spectrum of $[Ru(bpy)_3]^+$ were also observed. Figure 9 shows the transient spectrum recorded for Ru-SWCNT upon excitation at $\lambda = 490$ nm. The spectral temporal evolution did not allow a more detailed observation of the spectroscopic features expected for $[Ru(bpy)_3]^+$.

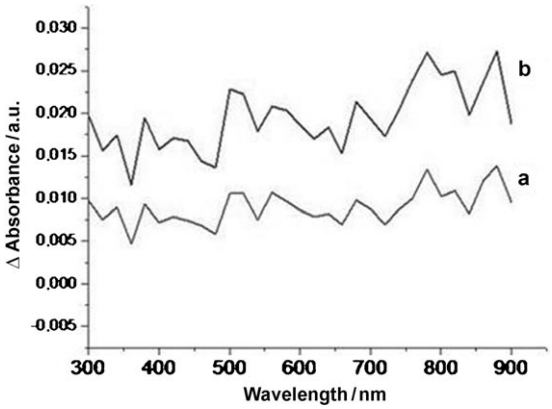

Figure 9. Transient spectrum from an N_2-purged aqueous solution of Ru-SWCNT ($70\,mL^{-1}$) recorded at a) 2.21 μs and b) 5.74 μs after laser excitation at $\lambda = 490$ nm.

Firm spectroscopic evidence of the formation of $[Ru(bpy)_3]^+$ could be obtained, however, using the $\lambda = 308$ nm pulses from an excimer laser. By using an excitation wavelength of $\lambda = 308$ nm, both $[Ru(bpy)_3]^{2+}$ triplets as negative signals corresponding to the emission from $\lambda = 550$ to 780 nm and the $[Ru(bpy)_3]^+$ absorption were clearly observed. In agreement with this assignment, the $\lambda = 480$–560 nm band, specific to $[Ru(bpy)_3]^+$, is not quenched by oxygen. Interestingly, a control in which a $[Ru(bpy)_3]^{2+}$ aqueous solution is photolyzed in the absence of SWCNT only shows the negative signal corresponding to the phosphorescence emission, whereas the signal at $\lambda = 360$ nm recorded for Ru-SWCNT exhibits some oxygen quenching with the same quenching rate constant ($k_q = 1.5 \times 10^6\,s^{-1}$) reported previously for $[Ru(bpy)_3]^{2+}$ triplets.[30] If a sufficiently high concentration of SWCNT is added to this $[Ru(bpy)_3]^{2+}$ solution, then the generation of $[Ru(bpy)_3]^+$ accompanying $[Ru(bpy)_3]^{2+}$ triplets is again observed. Figure 10 shows the transient spectra recorded upon excitation at $\lambda = 308$ nm of Ru-SWCNT, $[Ru(bpy)_3]^{2+}$, and a mixture of $[Ru(bpy)_3]^{2+}$ and SWCNT.

The experiments using excitation at $\lambda = 308$ nm prove the occurrence of photoinduced electron transfer from SWCNT to $[Ru(bpy)_3]^{2+}$ and that this process is strongly favored by the covalent attachment between $[Ru(bpy)_3]^{2+}$ and SWCNT.

We note, however, that the signal trace monitored at $\lambda = 360$ nm, upon excitation at 308 nm of Ru-SWCNT, was totally different to that previously recorded after a laser pulse at $\lambda = 490$ nm (see Figure 11). When using the $\lambda = 308$ nm laser, $[Ru(bpy)_3]^+$ is instantaneously formed upon excitation of Ru-SWCNT without the delayed formation observed at $\lambda = 490$ nm. These different temporal signal profiles, using $\lambda = 308$ or 490 nm lasers, indicate that the photochemistry arising from the $[Ru(bpy)_3]^{2+}$ MLCT band excitation at $\lambda = 440$ nm is more complex than the excitation at $\lambda = 308$ nm.

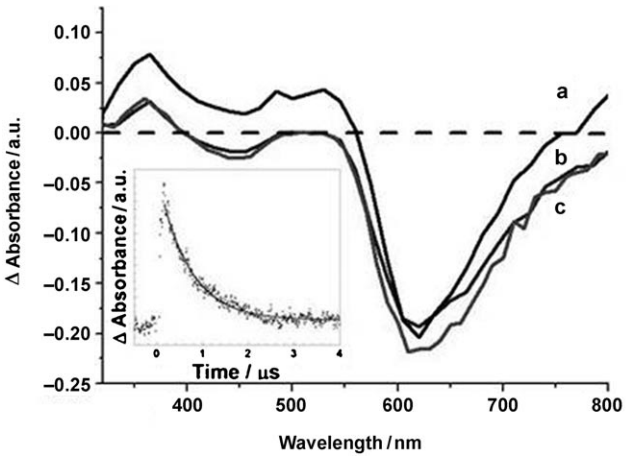

Figure 10. Transient spectrum recorded 500 ns after excitation at $\lambda = 308$ nm of an aqueous solution of a) Ru-SWCNT ($70\,mL^{-1}$), b) $[Ru(bpy)_3]^{2+}$, and c) a mixture of $[Ru(bpy)_3]^{2+}$ and SWCNT. The inset shows the temporal profile recorded at $\lambda_{em} = 360$ nm from the Ru-SWCNT aqueous solution upon laser excitation at 308 nm.

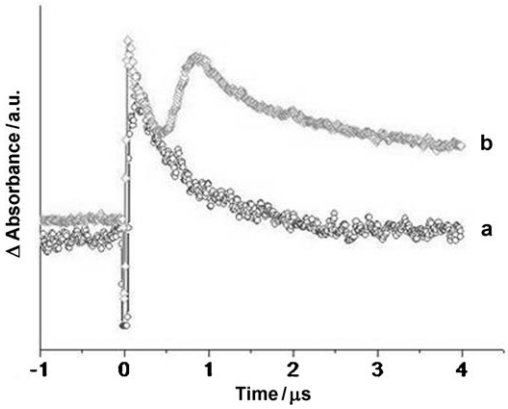

Figure 11. Normalized temporal profile of a deaereated aqueous solution of Ru-SWCNT ($70\,mL^{-1}$) recorded at $\lambda = 360$ nm using laser excitation at a) $\lambda = 308$ nm and b) 490 nm.

To understand the origin of the differences in the kinetics as a function of the excitation wavelength, we performed a laser-power dependence study of the signal intensity monitored at $\lambda = 360$ nm upon excitation at $\lambda = 490$ nm. Figure 12 reveals a remarkable influence of the laser flux on the shape of the signal temporal profile, and shows the ratio between the signal intensities measured at 1400 and 52 ns after the laser pulse. The ratio follows a quadratic relationship with the laser power, indicating that the delayed generation of $[Ru(bpy)_3]^+$ results from a two-photon process. Importantly, when an aqueous solution of $[Ru(bpy)_3]^+$ at the same concentration as in Ru-SWCNT is photolyzed under the same conditions and laser power as that in which the two-photon process for Ru-SWCNT is observed, no delayed $[Ru(bpy)_3]^+$

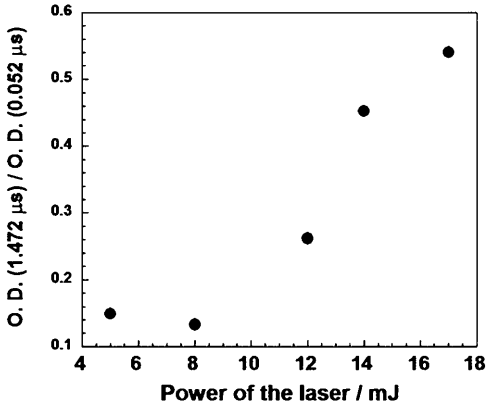

Figure 12. Ratio between the signal intensities (△O.D.) recorded at 1400 ns and 52 ns, monitoring at 360 nm upon 490 nm laser excitation of a deareated aqueous solution of Ru-SWCNT ($70\,mL^{-1}$) with increasing laser power.

growth is observed. This control experiment indicates that the SWCNT structure plays an active role in this process. The shape of this trace is reminiscent of those recorded previously with azaxanthyl-decorated SWCNT; unlike Ru-SWCNT in that case, however, the signal shape is insensitive to laser power, and is then attributed to a monophotonic process.[49]

Mechanistic proposal for the delayed $[Ru(bpy)_3]^+$ generation: The photochemistry of ruthenium polypyridyl complexes has been the subject of numerous studies and is well understood. The possible transient species includes a triplet excited state and the reduced $[Ru(bpy)_3]^+$ and oxidized $[Ru(bpy)_3]^{3+}$ ruthenium polypyridyl complexes.[30,49,50] On the other hand, it is also known that SWCNTs can behave as semiconductors, accepting or donating electrons.[51,52] The mobility of electron and holes in SWCNTs is also very large.[43] Based on this previous knowledge, we propose a plausible mechanism to rationalize the time-resolved spectroscopic study of Ru-SWCNT and particularly for how a two-photon process generates the delayed formation of $[Ru(bpy)_3]^+$. The proposal is summarized in Scheme 2. Notably, a study performed with the AZX-CNT sample reported in reference [41] shows that the temporal profile is independent of the laser power in the 5–14 mJ pulse^{-1} range.

As indicated in Scheme 2, excitation of the $[Ru(bpy)_3]^{2+}$ MLCT band by two sequential photons leads to the formation of two distant triplet $[Ru(bpy)_3]^{2+}$ excitons. A high-energy laser pulse, the long lifetime of $[Ru(bpy)_3]^{2+}$ triplets, and the low energy of the valence band in SWCNT increases the possibility of having simultaneously two $[Ru(bpy)_3]^{2+}$ triplets at different locations in the same SWCNT.

Initial electron transfer from one of these triplets to the SWCNT conduction band leads to $[Ru(bpy)_3]^{3+}$ and one electron localized on the SWCNT moiety (steps i and ii in Scheme 2). Electron migration of the electron on the SWCNT conduction band will move the electron close to the other triplet excited state. Electron transfer from the

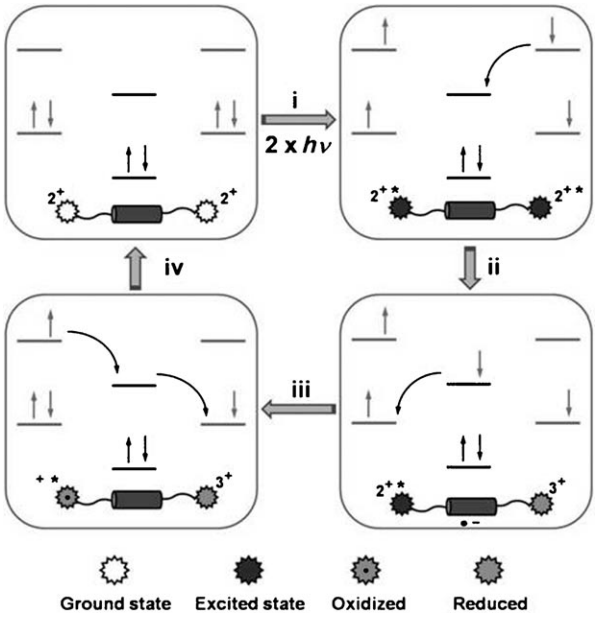

Scheme 2. Proposed mechanism for the biphotonic delayed formation of the $[Ru(bpy)_3]^+$. i) Two-photon absorption leading to the formation of two $[Ru(bpy)_3]^{2+}$ triplets; ii) electron transfer from a $[Ru(bpy)_3]^{2+}$ triplet to the LUMO of the SWCNT; iii) electron transfer from the LUMO of the SWCNT to the HOMO of $[Ru(bpy)_3]^{2+}$ triplet; iv) double electron transfer from $[Ru(bpy)_3]^+$ to $[Ru(bpy)_3]^{3+}$ mediated by the LUMO of the SWCNT.

SWCNT conduction band to the HOMO vacancy in the $[Ru(bpy)_3]^{2+}$ triplet will generate $[Ru(bpy)_3]^+$ (Scheme 2, iii). This $[Ru(bpy)_3]^+$ will be formed after some delay with respect to the laser pulse. In this way, SWCNT can act as an electron wire or electron relay in the disproportionation of two $[Ru(bpy)_3]^{2+}$ triplets in a process that illustrates its performance as a semiconductor. The spin selection rules have to be fulfilled in the process and, thus, it is likely that the two-photon process would require triplets with different spin angular momentum. It is also reasonable to assume that the first electron transfer from the $[Ru(bpy)_3]^{2+}$ triplet to the SWCNT is significantly faster than the second electron transfer from the SWCNT conduction band to the $[Ru(bpy)_3]^{2+}$ triplet, owing to the random electron migration through the nanotube. Thus, the growth observed in the delayed formation of $[Ru(bpy)_3]^+$ (region B in Figure 8) would correspond to the migration followed by the electron transfer from the SWCNT to the $[Ru(bpy)_3]^{2+}$ triplet. The relative kinetics of the electron injection into the SWCNT LUMO and subsequent electron transfer from the SWCNT LUMO to the $[Ru(bpy)_3]^{2+}$ triplet HOMO follows the trend found for these processes as in $[Ru(bpy)_3]^{2+}$-sensitized TiO_2 solar cells, in which the electron injection from the $[Ru(bpy)_3]^{2+}$ triplet into the TiO_2 conduction band takes place in the picosecond time scale, whereas recombination from the TiO_2 conduction band to the HOMO of $[Ru(bpy)_3]^{2+}$ occurs in the microsecond time scale.[53]

The mechanism outlined in Scheme 2 consists, essentially, of the disproportionation of two $[Ru(bpy)_3]^{2+}$ triplets medi-

ated by the SWCNT. This requires the formation of the oxidized $[Ru(bpy)_3]^{3+}$ and reduced $[Ru(bpy)_3]^{+}$ ruthenium complexes. As shown in Figure 10, excitation of Ru-SWCNT at $\lambda = 308$ nm provides spectroscopic evidence for the generation of $[Ru(bpy)_3]^{+}$, however, we have not been able to observe a transient spectrum compatible with the presence of $[Ru(bpy)_3]^{3+}$ upon excitation at $\lambda = 308$ or 430 to 530 nm. We propose two reasons for the failure to observe $[Ru(bpy)_3]^{3+}$: 1) The intense phosphorescence emission from $[Ru(bpy)_3]^{2+}$ triplets appearing in the same spectral zone as the MLCT band of $[Ru(bpy)_3]^{3+}$, thus masking any absorption for $[Ru(bpy)_3]^{3+}$. In addition, the two-photon process is not observed upon excitation at $\lambda = 308$ nm. 2) The interference of the SWCNT electron absorption when the excitation is carried out with the OPO laser from $\lambda = 430$ to 550 nm. Exciting at these wavelengths, even the observation of $[Ru(bpy)_3]^{+}$ is problematic. In this regard, there are precedents in the literature, in which the formation of $[Ru(bpy)_3]^{3+}$ has also been undetectable by laser flash photolysis due to similar interference.[47]

Conclusion

The study of ruthenium polypyridyl complexes attached to SWCNTs is of wide interest from the fundamental and applied point of view. In the present work we provide characterization data that supports the structural integrity and purity of a sample in which a ruthenium polypyridyl complex has been covalently attached to the carbon nanotube. The loading of this complex (15.6 wt %) is quite large in relation to the known precedents of covalent attachment through carboxylic acid groups in carbon nanotubes. We have found that the ruthenium complex triplet excited state is partially quenched by the SWCNTs and that the covalent tethering between the two components reinforces this interaction. Laser flash photolysis has revealed an unprecedented laser power dependence that indicates the occurrence of a unique two-photon mechanism that leads to the delayed generation of $[Ru(bpy)_3]^{+}$. We propose that this delayed formation occurs through the disproportionation of two $[Ru(bpy)_3]^{2+}$ triplets , which requires the participation of carbon nanotubes as electron relay. This process illustrates the unique properties of SWCNT-derived materials, which are distinctive from the response of the individual components.

In the context of solar-cell applications, it is very unlikely that the occurrence of the multiphotonic processes can take place in sunlight. However concerning the monophotonic process, as illustrated in Figure 10 for excitation at $\lambda =$ 308 nm, our study shows the formation of a triplet excited state accompanied by the expected photoinduced electron transfer processes with formation of $[Ru(bpy)_3]^{+}$ and $[Ru(bpy)_3]^{3+}$. Of these simultaneous electron transfer processes only one of them should be useful for the photovoltaic response. Therefore we expect the efficiency of Ru polypyridyl complexes and carbon nanotubes to be subject to much improvement, if the new derivatives triplet excited states all undergo electron transfer quenching to only one of the two redox states. In this way our photochemical data should prove useful in the design of more efficient SWCNT-based systems for solar cells.

Experimental Section

Materials and instrumentation: All ^{1}H NMR and ^{13}C NMR spectra were recorded in CD_3CN or $[D_6]$DMSO as solvents by using a Bruker 300 apparatus except for Ru-SWCNT, for which a Varian Gemini 400 MHz spectrometer was used. Chemical shifts are given in δ (ppm) using TMS as standard. UV/Vis absorption spectra were obtained in water using quartz cuvettes by means of a Shimadzu spectrophotometer. FT-IR spectra were recorded with a Nicolet Impact 410 spectrophotometer using KBr disks or self-supported wafers compressed to 2 Ton cm^{-2} for 2 min. XP spectra were recorded with a SPECS spectrometer equipped with a Phoibos 150 9MCD detector using a non-monochromatic X-ray source (Al and Mg) operating at 200 W. The samples were pressed into a small disc and evacuated in the pre-chamber of the spectrometer at 1×10^{-9} mbar. The measured intensity ratios of the components were obtained from the area of the corresponding peaks after nonlinear Shirley-type background subtraction and corrected by the transmission function of the spectrometer. Casa software was used for quantification and spectra treatment. The binding energy (BE) of the peaks was corrected by the charging effect. Single-walled carbon nanotube samples used in this study were obtained from "Chengdu Alpha Nano Technology Co., Ltd" and they have a relative carbonaceous purity $>90\,\%$, SSA >400 m^2 g^{-1}, and 5–20 μm length (supplier data). 4,4′-Dimethyl-2,2'-bipyridine, ruthenium dichloride, allyl bromide, oxalyl chloride, triethylamine, azobisisobutyronitrile (AIBN), thionyl chloride, amminoethanethiol, and all the anhydrous solvents were purchased from Sigma–Aldrich and used as received.

Photophysical studies: Laser flash photolysis experiments were carried out by using a LuzChem LFP-111 System and the fourth harmonic of a Nd/YAG laser (Surelite-II $\lambda = 266$ nm, 7 ns fwhp, 5 mJ pulse^{-1}) as excitation source. The samples were diluted up to an absorbance of around 0.15–0.20 units and then contained in 1×1 cm^2 cuvettes capped with septa, they were purged with N_2 or O_2 for at least 15 min before the measurements. For excitation, the forth harmonic (7 ns fwhh, 50 mJ pulse^{-1}) of the primary beam of a Nd-YAG laser or an Nd-YAG pumped OPO operating at different wavelengths from $\lambda = 430$ to 540 nm (7 ns fwhh, 8–14 mJ pulse^{-1}) were used. A Lumonics 535 excimer laser was used for excitation at $\lambda = 308$ nm ($\approx$10 ns fwhm, 20 mJ pulse^{-1}). The system was controlled by using a PC computer with LuzChem LFPv3 software.

Synthesis of 4-(3-butenyl)-4′-methyl-2,2′-bipyridine (2): A solution of 4,4′-dimethyl-2,2'-bipyridine (1 g, 5.43 mmol) in dry THF (45 mL) was added dropwise (15 min) at −78 °C under a nitrogen atmosphere, to a stirred solution of freshly prepared lithium diisopropylamide (LDA) [from *i*PrNH (0.8 mL, 5.6 mmol) and *n*BuLi (1.6 mol L^{-1} in hexane, 3.5 mL, 5.6 mmol) in dry THF (10 mL) at −78 °C]; this treatment resulted in a dark brown-red solution. The mixture was allowed to warm up to 0 °C before being stirred further at this temperature for 1 h. A solution of allyl bromide (0.72 g, 6.0 mmol) in dry THF (15 mL) was added dropwise, while the reaction mixture turned light yellow. After overnight stirring at room temperature, the redish solution was quenched with MeOH (5 mL) and the solvent removed in vacuo. The residue was dissolved in CH_2Cl_2, and the resulting solution was washed with H_2O and brine, and dried over $MgSO_4$. Removal of the solvent gave the crude product, which was submitted to column chromatography (SiO_2: silica gel as stationary phase—eluent: CH_2Cl_2/MeOH/NH_4OH, 100:1:0.2) to yield the bipyridine derivative **2** (0.88 g, 72 %) as a brownish oil. ^{1}H NMR (300 MHz, CD_3Cl): $\delta =$ 8.51 (d, $J = 4.8$ Hz, 1H; arom. H), 8.48 (d, $J = 5.1$ Hz, 1H; arom. H), 8.19 (s, 1H; arom. H), 8.17 (s, 1H; arom. H), 7.07 (d, $J = 5.1$ Hz, 2H; arom. H), 5.79 (m, 1H; vinyl. H), 4.99 (d, $J = 19.5$H, 1H; vinyl. H), 4.95 (d, $J =$ 13.2 Hz, 1H; vinyl. H), 2.74 (t, $J = 8.4$ Hz, 2H), 2.41 (t, $J = 6.9$ Hz, 2H),

2.37 ppm (s, 3H; CH3); ^{13}C NMR (300 MHz, CD_3Cl): $\delta = 155.67$, 155.52, 148.54, 148.44, 147.58, 136.67, 124.20, 123.47, 121.59, 120.86, 115.17, 34.34, 33.80, 20.69 ppm; IR (KBr): $\tilde{\nu} = 2924$, 2858, 1935, 1710, 1602, 1552, 1378, 1261, 1103, 988, 921, 830, 655, 563, 514 cm^{-1}; GC-MS: *m/z*: calcd for $C_{15}H_{16}N_2^+$ ($[M]^+$) 224.13; found: 223 ($[M^+ - H]$).

Synthesis of 4-(3-butenyl)-4′-methyl-2,2′-bipyridine-2,2′-bipyridine ruthenium(II) bishexafluorophosphate (3): A mixture of $[Ru(bpy)_2]Cl_2$ (**1**; 1.2 g, 2.46 mmol) and bipyridine (**2**; 0.5 g, 2.23 mmol) in $EtOH/H_2O$ (60 mL, 3:1 v/v) was heated under reflux and an N_2 atmosphere for 24 h. After removal of the solvent, the residue was purified by column chromatography (silica gel using as eluent a $MeOH/NH_4Cl$ (2 mol L^{-1})/$MeNO_2$, 7:2:1 mixture). Fractions containing the product were collected and concentrated in vacuo. The residue was treated with an excess of 50% aqueous NH_4PF_6 solution. The red solid was filtered off, washed with Et_2O, and dried in vacuo to obtain the bishexafluorophosphate Ru^{II}–butenyl complex **3** (1.14 g, 55%). ^{1}H NMR (300 MHz, CD_3Cl): $\delta = 8.51$ (d, $J =$ 4.8 Hz, 1H; arom. H), 8.48 (d, $J = 5.1$ Hz, 1H; arom. H), 8.19 (s, 1H; arom. H), 8.17 (s, 1H; arom. H), 7.07 (d, $J = 5.1$ Hz, 2H; arom. H), 5.79 (m, 1H; vinyl. H), 4.99 (d, $J = 19.5$ H, 1H; vinyl. H), 4.95 (d, $J = 13.2$ Hz, 1H; vinyl. H), 2.74 (t, $J = 8.4$ Hz, 2H), 2.41 (t, $J = 6.9$ Hz, 2H), 2.37 ppm (s, 3H; CH_3); ^{13}C NMR (300 MHz, CD_3CN): $\delta = 157.57$, 157.10, 156.99, 154.30, 152.19, 152.01, 151.95, 151.41, 151.25, 150.96, 138.10, 137.48, 128.78, 128.14, 127.99, 125.46, 124.80, 124.69, 115.94, 34.49, 34.07, 20.73 ppm; IR (KBr): $\tilde{\nu} = 3655$, 3580, 3440, 3098, 2932, 2866, 1976, 1619, 1436, 1312, 1245, 1162, 1020, 854, 754, 646, 555, 422 cm^{-1}; HR-FAB-MS: *m/z*: calcd for $[C_{35}H_{32}N_6Ru]P_2F_{12}^+$ ($[M]^+$) 928.1; found: 782.223 ($[M^+ - PF_6]$), 637.099 ($[M^+ - 2PF_6]$).

Purification and shortening of commercial HiPCO SWCNT: This procedure is a pre-treatment process because it can only remove the catalyst particles. The obtained material was used as the initial material for the following procedures. A 1 g sample of commercially available high-pressure carbon monoxide (HiPCO) single-walled carbon nanotubes (SWCNTs) was refluxed in HNO_3 (500 mL; 3 M) for 12 h; a reaction temperature of 120 °C was optimized in our experiment. Then, the black suspension was diluted with distilled water and cooled to room temperature. Five cycles of centrifugation–redispersion in Milli-Q water were carried out to remove the excess acid, until the pH of the filtrate was neutral. Finally, the carbonaceous material was submitted to freeze vacuum overnight to obtain a black dustlike material. The efficiency of the process was corroborated by TG analysis. Purified HiPCO SWCNTs were cut by an ultrasonication/heating method using a mixture of acids. An acid solution comprising a 3:1 (v/v) mixture of 96% H_2SO_4 and 30% HNO_3 was prepared immediately prior to use. Then, purified SWCNT (150 mg) was sonicated at 60 °C in the acid mixture (8 mL) for 45–60 min. After this time, several cycles of centrifugation–redispersion in Milli-Q water were performed until the pH of the solution was neutral and finally the suspension was freeze-dried to obtain the soluble, short SWNT as residue. The average length of the shortened SWCNT is 500 nm (estimated by TEM).

Synthesis of SH-SWCNT: Chlorination of SWCNTs to transform carboxylic acid groups into acyl chlorides was carried out after purification and cutting of commercial SWNT. Then, the resulting sample (500 mg) was first sonicated in anhydrous DMF (60 mL) to give a homogeneous suspension and subsequently thionyl chloride (1.5 mL) was added dropwise to the SWNT suspension at 0 °C under N_2. The mixture was stirred at 0 °C for 2 h and then at room temperature for an additional 2 h. Finally, the temperature was raised to 70 °C, and the mixture was stirred overnight. The excess of thionyl chloride was removed in vacuo, and the black material suspended in CH_2Cl_2. The chlorinated SWCNT-COCl sample was collected by filtration through a PTFE membrane (pore size 0.2 μm) and then re-dispersed in anhydrous DMF (60 mL). The mercaptoethylamide-functionalized SH-SWCNTs were obtained by adding a solution of aminoethanethiol in DMF into the dispersion of SWCNT-COCl and heating overnight with magnetic stirring at 90 °C. The sample was purified by consecutive centrifugation/redispersion cycles and final freeze-drying.

Preparation of Ru-SWCNT: Argon-purged anhydrous acetonitrile (5 mL) was added to a mixture of the vinyl derivative of ruthenium polypyridyl complex **3** (50 mg), AIBN (20 mg), and mercaptoethylamido-functionalized SH-SWCNT (100 mg) and the mixture was sonicated for 1 h to obtain a black dispersion. Then, the suspension was stirred at reflux under an argon atmosphere for 48 h. After this time the reaction mixture was diluted with acetonitrile and filtered through a 0.2 μm PTFE membrane. The isolated black material was washed exhaustively several times with acetonitrile, redispersed in acetonitrile by sonication, and finally centrifuged at 15000 rpm for 2 h. After this time, the solvent was decanted and the Ru-SWCNT sample was washed again with a mixture of toluene and diethyl ether (10:1). The samples were then vacuum dried at 30 °C for one day. The functionalized nanotubes were quite soluble in DMSO, giving a dark solution.

Acknowledgements

Financial support by the Canadian NSERC (J.C.S. Discovery grant) and Spanish MICINN (H.G., CTQ2009-11583 and M.A., CTQ2007-67805/PPQ) is gratefully acknowledged. R.M. thanks the Spanish MICINN for a postgraduate scholarship.

[1] D. Tasis, N. Tagmatarchis, A. Bianco, M. Prato, *Chem. Rev.* **2006**, *106*, 1105–1136.
[2] L. W. Qu, R. B. Martin, W. J. Huang, K. F. Fu, D. Zweifel, Y. Lin, Y. P. Sun, C. E. Bunker, B. A. Harruff, J. R. Gord, L. F. Allard, *J. Chem. Phys.* **2002**, *117*, 8089–8094.
[3] S. Campidelli, B. Ballesteros, A. Filoramo, D. D. G. Diaz de La Torre, T. Torres, G. M. A. Rahman, C. Ehli, D. Kiessling, F. Werner, V. Sgobba, D. M. Guldi, C. Cioffi, M. Prato, J. P. Bourgoin, *J. Am. Chem. Soc.* **2008**, *130*, 11503–11509.
[4] A. Krueger, *Chem. Eur. J.* **2008**, *14*, 1382–1390. R. A. Hatton, A. J. Miller, S. R. P. Silva, *J. Mater. Chem.* **2008**, *18*, 1183–1192.
[5] V. Sgobba, D. M. Guldi, *Chem. Soc. Rev.* **2009**, *38*, 165–184.
[6] V. Sgobba, D. M. Guldi, *J. Mater. Chem.* **2008**, *18*, 153–157.
[7] D. M. Guldi, G. M. A. Rahman, M. Prato, N. Jux, S. H. Qin, W. Ford, *Angew. Chem.* **2005**, *117*, 2051–2054; *Angew. Chem. Int. Ed.* **2005**, *44*, 2015–2018.
[8] T. Hasobe, S. Fukuzumi, P. V. Kamat, *J. Phys. Chem. B* **2006**, *110*, 25477–25484.
[9] N. Ikeda, T. Miyasaka, *Chem. Lett.* **2007**, *36*, 466–467.
[10] S. R. Jang, R. Vittal, K. J. Kim, *Langmuir* **2004**, *20*, 9807–9810.
[11] A. Kongkanand, R. M. Dominguez, P. V. Kamat, *Nano Lett.* **2007**, *7*, 676–680.
[12] B. J. Landi, R. P. Raffaelle, S. L. Castro, S. G. Bailey in *Single-wall carbon nanotube-polymer solar cells*, 18th Space Photovoltaic Research and Technology (SPRAT 18), Cleveland, **2003**, 165–172.
[13] A. F. Nogueira, B. S. Lomba, M. A. Soto-Oviedo, C. R. D. Correia, P. Corio, C. A. Furtado, I. A. Hummelgen, *J. Phys. Chem. C* **2007**, *111*, 18431–18438.
[14] T. Umeyama, H. Imahori, *Energy Environ. Sci.* **2008**, *1*, 120–133.
[15] E. Kymakis, G. A. J. Amaratunga, *Appl. Phys. Lett.* **2002**, *80*, 112–114.
[16] E. Kymakis, G. A. J. Amaratunga, *Sol. Energy Mater. Sol. Cells* **2003**, *80*, 465–472.
[17] B. J. Landi, S. L. Castro, C. M. Evans, H. J. Ruf, S. G. Bailey, R. P. Raffaelle, Symposium on Materials for Photovoltaics, Fall Meeting of the MRS, Boston, **2004**, 55–60.
[18] N. Robertson, *Angew. Chem.* **2006**, *118*, 2398–2405; *Angew. Chem. Int. Ed.* **2006**, *45*, 2338–2345.
[19] A. Hagfeldt, M. Gratzel, *Acc. Chem. Res.* **2000**, *33*, 269–277.
[20] Y. M. Cao, Y. Bai, Q. J. Yu, Y. M. Cheng, S. Liu, D. Shi, F. F. Gao, P. Wang, *J. Phys. Chem. C* **2009**, *113*, 6290–6297.
[21] C. Y. Chen, S. J. Wu, C. G. Wu, J. G. Chen, K. C. Ho, *Angew. Chem.* **2006**, *118*, 5954–5957; *Angew. Chem. Int. Ed.* **2006**, *45*, 5822–5825.
[22] Z. Jin, H. Masuda, N. Yamanaka, M. Minami, T. Nakamura, Y. Nishikitani, *J. Phys. Chem. C* **2009**, *113*, 2618–2623.

[23] F. Matar, T. H. Ghaddar, K. Walley, T. DosSantos, J. R. Durrant, B. ORegan, *J. Mater. Chem.* **2008**, *18*, 4246–4253.
[24] K. Willinger, K. Fischer, R. Kisselev, M. Thelakkat, *J. Mater. Chem.* **2009**, *19*, 5364–5376.
[25] Q. J. Yu, S. Liu, M. Zhang, N. Cai, Y. Wang, P. Wang, *J. Phys. Chem. C* **2009**, *113*, 14559–14566.
[26] L. Kavan, O. Frank, M. Kalbac, L. Dunsch, *J. Phys. Chem. C* **2009**, *113*, 2611–2617.
[27] L. Kavan, S. M. Zakeeruddin, I. Exnar, M. Graetzel, *J. Electrochem. Soc.* **2009**, *156*, K44K50.
[28] K. H. Jung, S. R. Jang, R. Vittal, V. D. Kim, K. J. Kim, *Bull. Korean Chem. Soc.* **2003**, *24*, 1501–1504.
[29] K.-H. Jung, J. S. Hong, R. Vittal, K.-J. Kim, *Chem. Lett.* **2002**, 864–865.
[30] V. Balzani, A. Juris, *Coord. Chem. Rev.* **2001**, *211*, 97–115.
[31] V. Sgobba, G. M. A. Rahman, D. M. Guldi, *Chem. Carbon Nanotubes* **2008**, *2*, 109–147.
[32] C. Aprile, R. Martin, M. Alvaro, H. Garcia, J. C. Scaiano, *Chem. Mater.* **2009**, *21*, 884–890.
[33] K. H. Jung, S. R. Jang, R. Vittal, V. D. Kim, K. J. Kim, *Bull. Korean Chem. Soc.* **2003**, *24*, 1501–1504.
[34] J. Li, L.-R. Guo, W. Gao, X.-H. Xia, L.-M. Zheng, *Chem. Commun.* **2009**, 7545–7547.
[35] C. Baleizão, H. Garcia, *Chem. Rev.* **2006**, *106*, 3987–4043.
[36] P. McMorn, G. J. Hutchings, *Chem. Soc. Rev.* **2004**, *33*, 108–133.
[37] J. L. Hudson, M. J. Casavant, J. M. Tour, *J. Am. Chem. Soc.* **2004**, *126*, 11158–11159.
[38] H. Murakami, N. Nakashima, *J. Nanosci. Nanotechnol.* **2006**, *6*, 16–27.
[39] N. Tagmatarchis, M. Prato, D. M. Guldi, *Phys. E* **2005**, *29*, 546–550.
[40] D. Tasis, N. Tagmatarchis, V. Georgakilas, M. Prato, *Chem. Eur. J.* **2003**, *9*, 4000–4008.
[41] M. Alvaro, C. Aprile, B. Ferrer, H. Garcia, *J. Am. Chem. Soc.* **2007**, *129*, 5647–5655.
[42] C. Aprile, R. Martin, M. Alvaro, J. C. Scaiano, H. Garcia, *Chem. Eur. J.* **2008**, *14*, 5030–5038.
[43] R. Martín, L. B. Jimenez, M. Alvaro, J. C. Scaiano, H. Garcia, *Chem. Eur. J.* **2009**, *15*, 8751–8759.
[44] K. Chichak, N. R. Branda, *Chem. Commun.* **1999**, 523–524.
[45] D. J. Cárdenas, J.-P. Collin, P. Gavina, J.-P. Sauvage, A. De Cian, J. Fischer, N. Armaroli, L. Flamigni, V. Vicinelli, V. Balzani, *J. Am. Chem. Soc.* **1999**, *121*, 5481–5488.
[46] S. Campagna, F. Puntoriero, F. Nastasi, G. Bergamini, V. Balzani, *Top. Curr. Chem.* **2007**, *280* 117–214.
[47] V. Balzani, G. Bergamini, S. Campagna, F. Puntoriero, *Top. Curr. Chem.* **2007**, *280*, 1–36.
[48] A study performed here with the AZX-CNT sample reported in reference [32] shows that the temporal profile is independent of the laser power in the 5–14 mJ pulse^{-1} range in contrast to the shape changes presented in Figure 8 and 11 observed for Ru-SWCNT.
[49] V. Balzani, *Tetrahedron* **1992**, *48*, 10443–10514.
[50] R. Bensasson, C. Salet, V. Balzani, *J. Am. Chem. Soc.* **1976**, *98*, 3722–3724.
[51] B. Ballesteros, G. de La Torre, C. Ehli, G. M. A. Rahman, F. Agullo-Rueda, D. M. Guldi, T. Torres, *J. Am. Chem. Soc.* **2007**, *129*, 5061–5068.
[52] D. M. Guldi, G. M. A. Rahman, F. Zerbetto, M. Prato, *Acc. Chem. Res.* **2005**, *38*, 871–878.
[53] M. Gratzel, *J. Photochem. Photobiol. C* **2003**, *4*, 145–153.

Received: December 21, 2009
Revised: March 3, 2010
Published online: May 12, 2010

